

## Metal-insulator transition in NiS<sub>2</sub>-xSex

Jan Kuneš, L. Baldassarre, B. Schächner, Kaneez Rabia, Christine A. Kuntscher, Dm. M. Korotin, V. I. Anisimov, J. A. McLeod, E. Z. Kurmaev, A. Moewes

### Angaben zur Veröffentlichung / Publication details:

Kuneš, Jan, L. Baldassarre, B. Schächner, Kaneez Rabia, Christine A. Kuntscher, Dm. M. Korotin, V. I. Anisimov, J. A. McLeod, E. Z. Kurmaev, and A. Moewes. 2010. "Metal-insulator transition in NiS<sub>2</sub>-xSex." *Physical Review B* 81 (3): 035122. <https://doi.org/10.1103/physrevb.81.035122>.

**Metal-insulator transition in NiS<sub>2-x</sub>Se<sub>x</sub>**J. Kuneš,<sup>1,2,\*</sup> L. Baldassarre,<sup>3</sup> B. Schächner,<sup>3</sup> K. Rabia,<sup>3</sup> C. A. Kuntscher,<sup>3</sup> Dm. M. Korotin,<sup>4</sup> V. I. Anisimov,<sup>4</sup> J. A. McLeod,<sup>5</sup> E. Z. Kurmaev,<sup>4</sup> and A. Moewes<sup>4</sup><sup>1</sup>*Theoretical Physics III, Center for Electronic Correlations and Magnetism, Institute of Physics, University of Augsburg, Augsburg 86135, Germany*<sup>2</sup>*Institute of Physics, Academy of Sciences of the Czech Republic, Cukrovarnická 10, 162 53 Praha 6, Czech Republic*<sup>3</sup>*Experimental Physics II, Institute of Physics, University of Augsburg, Augsburg 86135, Germany*<sup>4</sup>*Institute of Metal Physics, Russian Academy of Sciences–Ural Division, 620041 Yekaterinburg GSP-170, Russia*<sup>5</sup>*Department of Physics and Engineering Physics, University of Saskatchewan,**116 Science Place, Saskatoon, Saskatchewan, Canada S7N 5E2*

(Received 27 October 2009; published 28 January 2010)

The origin of the gap in NiS<sub>2</sub> as well as the pressure- and doping-induced metal-insulator transition in the NiS<sub>2-x</sub>Se<sub>x</sub> solid solutions are investigated both theoretically using the first-principles band structures combined with the dynamical mean-field approximation for the electronic correlations and experimentally by means of infrared and x-ray absorption spectroscopies. The bonding-antibonding splitting in the S-S (Se-Se) dimer is identified as the main parameter controlling the size of the charge gap. The implications for the metal-insulator transition driven by pressure and Se doping are discussed.

DOI: [10.1103/PhysRevB.81.035122](https://doi.org/10.1103/PhysRevB.81.035122)

PACS number(s): 71.30.+h, 62.50.-p, 78.30.-j

**I. INTRODUCTION**

The metal-insulator transition (MIT) due to electronic correlations has been subject of intense research for several decades. The NiS<sub>2-x</sub>Se<sub>x</sub> series provided an important model system exhibiting a MIT controlled by varying the Se content  $x$ , temperature  $T$ , or pressure  $P$ .<sup>1-5</sup> Particularly interesting is the similarity of the  $x-T$  (Refs. 2 and 3) and  $P-T$  phase diagrams<sup>5</sup> to that of the Hubbard model in the infinite dimension limit,<sup>6</sup> consisting in the presence of the phase transition between paramagnetic metal and paramagnetic insulator at intermediate temperatures, existence of the high-temperature crossover regime, and the possibility of driving a metal insulating, in a certain range of  $x$ , by increasing the temperature. Consequently, the MIT has been commonly attributed to broadening of the Ni- $d$  band.<sup>3-5,7-9</sup> Despite a large volume of available experimental data, the microscopic origin of the MIT in NiS<sub>2-x</sub>Se<sub>x</sub> is poorly understood and a satisfactory material-specific theory is missing.

NiX<sub>2</sub> ( $X=S, Se$ ) can be viewed as NiO with the O atom replaced by an X<sub>2</sub> dimer. Strong hybridization between the  $X-p$  orbitals pointing along the  $X-X$  dimer,  $p_\sigma$  orbitals, leads to a formation of split bonding and antibonding bands (the latter ones are referred to as  $p_\sigma^*$ ), which accommodate two holes leading to an  $X_2^{-2}$  valence state. Numerous photoemission (PES) studies<sup>7,10,11</sup> complemented by cluster calculations<sup>7</sup> revealed a similarity between the NiX<sub>2</sub> and NiO valence-band (VB) spectra, supporting this analogy. The band-structure calculations in the local-density approximation (LDA) (Refs. 8, 12, and 13) rendered NiS<sub>2</sub> a metal with a partially filled  $e_g$  band and empty  $p_\sigma^*$  orbitals. By analogy to NiO, it was speculated that local  $d-d$  correlations open a gap between the S- $p$  band and the upper Hubbard band of Ni- $d$   $e_g$  character,<sup>8</sup> leading to the classification of NiS<sub>2</sub> as a charge-transfer (CT) insulator in the Zaanen-Sawatzky-Allen (ZSA) scheme,<sup>14</sup> although in the original ZSA paper NiS<sub>2</sub> was classified as “ $p$ -type metal were it not for the gap between the S  $p_\sigma^*$  and the rest of the  $p$  band.”

We have combined theoretical calculations with new experimental data in order to address the following questions: (i) Why is NiS<sub>2</sub> an insulator and NiSe<sub>2</sub> a metal? (ii) How do NiX<sub>2</sub> respond to external pressure? (iii) Are the effects of pressure and varying Se content equivalent? (iv) What is the mechanism of the MIT in NiS<sub>2-x</sub>Se<sub>x</sub>? The electronic structure of NiX<sub>2</sub> is studied numerically, using a combination of the *ab initio* band structure, obtained in the local-density approximation, and the dynamical mean-field theory (LDA + DMFT).<sup>6,15</sup> The infrared (IR) reflectivity is measured on samples with various Se concentrations under applied pressure to investigate the evolution of the optical gap and the spectral weight transfer. The x-ray absorption spectroscopy (XAS) at S  $K$  edge is used to elucidate the orbital character of features in the single-particle spectrum of NiS<sub>2</sub>.

**II. COMPUTATIONAL METHOD**

Our computations proceed as follows. First, we perform paramagnetic LDA calculations<sup>16</sup> and minimize the total energy to find the equilibrium S (Se) positions. Next, we represent the one-particle Hilbert space of the hybridized Ni- $d$  and S(Se)- $p$  bands in Wannier basis (44 orbitals per unit cell) and calculate the parameters of the on-site  $d-d$  interaction with the constraint LDA approach.<sup>17,18</sup> We found only moderately different  $U_{\text{NiS}_2}=5$  eV and  $U_{\text{NiSe}_2}=4.7$  eV and used  $J$  of 1 eV throughout the study. Finally, we construct a multi-band Hubbard Hamiltonian

$$\hat{H} = \sum_k \hat{\mathbf{a}}_k^\dagger \mathbf{H}_k \hat{\mathbf{a}}_k - \varepsilon_{dc}(n_d) \hat{N}_d + \sum_{i \in \text{Ni}} \hat{\mathbf{n}}_i^d \mathbf{U}^{dd} \hat{\mathbf{n}}_i^d \quad (1)$$

and compute the single-particle spectra using the DMFT approximation. Here,  $\mathbf{H}_k$  is the LDA Hamiltonian,  $44 \times 44$  matrices (four NiX<sub>2</sub> units) in the basis of Ni- $d$  and  $X-p$  Wannier orbitals, on a uniform  $k$  mesh in the first Brillouin zone.<sup>17</sup> The second term is the double-counting correction amount-

ing to a constant shift applied to Ni- $d$  site energies.<sup>19</sup> The last term is the two-particle interaction at the Ni sites in the density-density approximation. The DMFT equations are solved on the Matsubara contour. The continuous time quantum Monte Carlo impurity solver<sup>20</sup> is employed to solve the auxiliary multiorbital impurity problem. Single-particle spectral densities are obtained by analytic continuation of Monte Carlo data using the maximum entropy method.<sup>21</sup>

### III. EXPERIMENTAL DETAILS

Single crystals, grown by vapor transport technique, were slightly polished in order to obtain a clean, mirrorlike surface. Near-normal incidence reflectivity was measured with a cassegrainian-based IR microscope (Bruker IRscope II) coupled to a Michelson interferometer. The  $\text{NiS}_{2-x}\text{Se}_x$  series ( $x=0, 0.3, 0.5, 0.7$ ) was studied at ambient conditions.

A clamp diamond-anvil cell (Diacell cryoDAC-Mega) equipped with type-IIa diamonds was employed to perform pressure dependent studies. A small piece of  $\text{NiS}_2$  ( $\text{NiS}_{1.7}\text{Se}_{0.3}$ ) was cut and placed together with CsI (as hydrostatic pressure medium) inside a 400  $\mu\text{m}$  hole drilled in a 90- $\mu\text{m}$ -thick CuBe gasket. The pressure was evaluated *in situ* by the standard ruby-fluorescence technique.<sup>23</sup> Measurements were carried out partly at the University of Augsburg and partly at the IR1 beamline at ANKA so to exploit the high brilliance of synchrotron radiation in the far-IR range. We recall that due to the small size of the samples inside the diamond-anvil cell, measurements as a function of pressure were performed for  $\omega > 250 \text{ cm}^{-1}$ . The measurement procedure, as well as the data processing to extract the optical conductivity  $\sigma_1(\omega)$ , are carefully described in Refs. 24 and 25.

The sulfur  $1s$  XAS which provides information about vacant S  $3p$  states were measured at the soft x-ray microcharacterization beamline (SXRMB) at the Canadian Light Source. The spectra were measured in total electron yield (TEY) mode. Additional measurements were taken in total fluorescence yield (TFY) mode using a channel-plate detector and partial fluorescence yield (PFY) mode using a silicon drift detector with a resolution of about 100 eV. Both the PFY and TFY measurements showed the same features as the TEY measurements, indicating that the surface of the samples was clean. The TEY measurements were used for the analysis because they had a better signal-to-noise ratio than the TFY or PFY measurements and did not suffer from the self-absorption effects present in the fluorescence measurements. An Si(111) crystal was used in the monochromator and the experimental resolution ( $E/E$ ) was about 10000.

### IV. RESULTS AND DISCUSSION

We start the exposition of our results with a brief review of the noninteracting LDA band structures, which agree with those published previously.<sup>8,12,13</sup> The Ni- $d$  orbitals form narrow  $t_{2g}$  and broader, Ni- $X$  antibonding,  $e_g^\sigma$  bands due to octahedral coordination of Ni with the chalcogen  $X$ . The deviations from an exact octahedral symmetry at the Ni sites lead

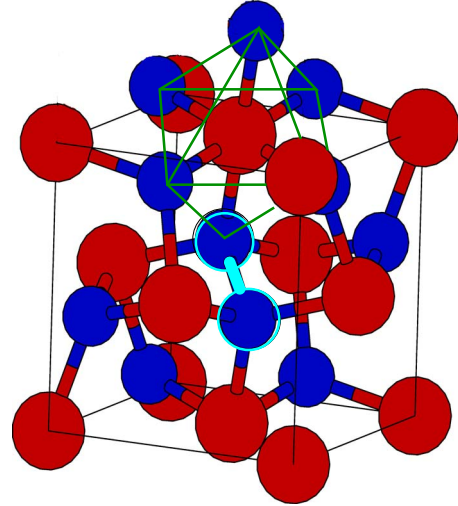


FIG. 1. (Color online) The crystal structure of  $\text{NiS}_2$ : Ni atoms red (bright), S atoms blue (dark). The S-S dimer is highlighted in the center of the figure.

to further splitting of the  $t_{2g}$  bands into an  $e_g^\pi$  doublet and an  $a_{1g}$  singlet. This splitting plays no discernible role in our investigation. The characteristic feature of the chalcogen bands is a large bonding-antibonding splitting of the  $p$  orbitals pointing along the  $X-X$  dimer (Fig. 1). Due to the S-S-Ni angle being close to the right angle ( $\approx 104^\circ$  in  $\text{NiS}_2$ ), the dimer states hybridize only weakly with the Ni  $e_g^\sigma$  states.

The Ni- $X$  and  $X-X$  dimer distances as function of the lattice constant were obtained by minimization of the LDA total energies (see Fig. 2). At ambient pressure, the calculated  $\text{NiS}_2$  bond lengths agree well with experimental observations. Compression leads to shortening of the Ni-S distance while the S-S dimer behaves as a rigid object. The situation is less clear in  $\text{NiSe}_2$ . While the calculated ambient pressure Ni-Se bond length reproduces the experimental value, the length of the Se-Se dimer is substantially overestimated. Under pressure, our calculations yield an initial increase of the

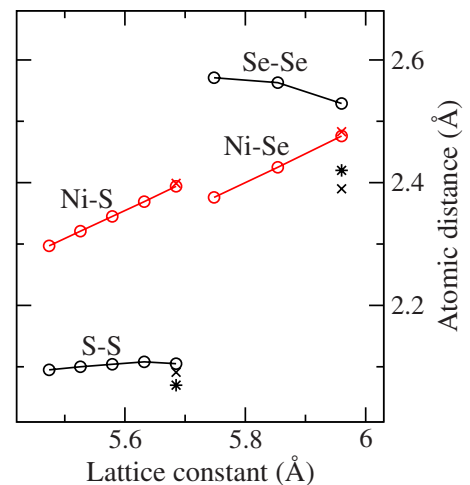


FIG. 2. (Color online) The calculated pressure dependence of the equilibrium Ni- $X$  and  $X-X$  distances. The isolated points mark the experimental values of Refs. 11 (star) and 27 (cross).

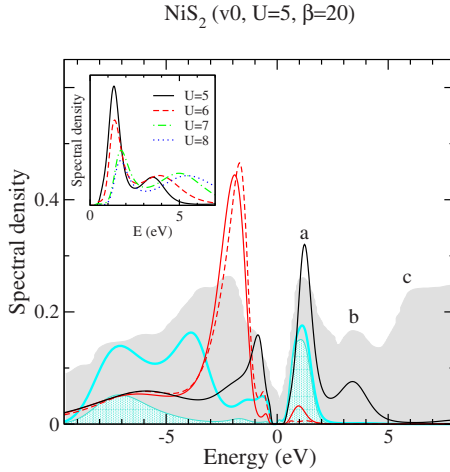


FIG. 3. (Color online) The calculated ( $U=5$  eV,  $T=580$  K) orbitally resolved spectra of  $\text{NiS}_2$  [ $\text{Ni-d}: e_g^\sigma$  (black) and  $t_{2g}=e_g^\pi$  (red) +  $a_{1g}$  (red dashed);  $\text{S-p}$ : total (blue, thick) and  $p_\sigma$  (blue shaded)] compared to the experimental XPS+BIS (gray, shaded) (Ref. 11). *a*, *b*, and *c* are defined in the text. Inset shows the conduction-band  $e_g^\sigma$  spectra for  $U=5, 6, 7$ , and  $8$  eV.

Se-Se distance indicating that the Ni-Se bond becomes stronger relative to the Se-Se bond and suggesting that Se-Se dimer cannot be viewed as a molecular unit. We will discuss later on how the behavior of the bond lengths affects the electronic properties).

## A. Single-particle spectra

### 1. $\text{NiS}_2$

In this section, we present orbitally resolved spectral densities obtained at ambient pressure with the LDA+DMFT method. In Fig. 3, we show the  $\text{NiS}_2$  spectra, which exhibit a small charge gap in agreement with experimental observations. The VB resembles that of  $\text{NiO}$  (Ref. 26) with the characteristic distribution of the Ni- $d$  spectral weight between  $d^7$  (around  $-6$  eV) and  $d^8L$  excitations (at low binding energy), the result of a strong  $p-e_g^\sigma$  hybridization. Overall, a good correspondence between positions of the main features in the experimental x-ray photoemission spectra (XPS) and their theoretical counterparts can be stated. Particularly important for the further discussion is the high-energy shoulder at  $-7$  eV, which is dominated by the  $\text{S-p}$  density in agreement with the observation of Ref. 10. The absence of an obvious gap in the experimental spectra shown in Fig. 3 is due to the experimental resolution.

The calculated conduction-band (CB) spectrum consists of two peaks: (a)  $p_\sigma^*$  band with a large resonant  $e_g^\sigma$  contribution at 1 eV and (b) the upper Hubbard band of pure  $e_g^\sigma$  character at 3.5 eV. The identification of (b) with the upper Hubbard band is based on the observation of its shift upon increasing the interaction strength (see the inset of Fig. 3) and the absence of  $p$  character. The experimental CB spectrum, obtained with the Bremsstrahlung isochromat spectroscopy (BIS) of Ref. 11, exhibits three distinct features: a sharp low-energy peak at 1 eV, a high-energy peak at 3.5 eV, and a broad band (c) starting around 5.5 eV. The 5.5 eV band is not

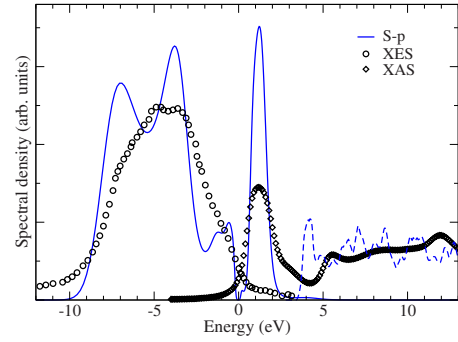


FIG. 4. (Color online) The calculated  $\text{S-p}$  spectral density obtained from LDA+DMFT (full line), augmented with the  $\text{S-p}$  contribution from the high energy LDA bands (dashed line), compared to experimental XES spectra of Ref. 28 (circles) and XAS (diamonds) spectra of this work.

spanned by the Hamiltonian (1) and thus the corresponding contribution is missing in Fig. 3. The orbital character of the other two peaks is of key importance for understanding the nature of the charge gap. The question can be formulated simply as “is the upper Hubbard band located below or above the  $p_\sigma^*$  band?” The authors of Ref. 11 interpreted the 1 eV peak as Ni- $d$  upper Hubbard band and the 3.5 eV peak as  $\text{S } p_\sigma^*$  band, which is in clear contradiction to our result.

In order to resolve this issue, we have measured the XAS at the  $K$  edge of sulfur, which can be directly compared to the calculated  $\text{S-p}$  spectral density as shown in Fig. 4. The theoretical high-energy spectrum was obtained by projecting the  $\text{S-p}$  contribution from the LDA bands not included in the Hamiltonian (1). The identification of peak (a) with  $p_\sigma^*$  is corroborated by its position with respect to the x-ray emission (XES) spectrum as well as by its distance from the high energy (5 eV) XAS band. Although the calculated onset of the high-energy band is misplaced by about 1 eV with respect to the experiment, the overall agreement is very good. We point out that the experimental XAS (a) and (c) peaks match their BIS counterparts perfectly.

### 2. $\text{NiSe}_2$

The LDA+DMFT calculations yield  $\text{NiSe}_2$  metallic. Its low-energy spectrum is rather sensitive to changes of  $U$ , as shown in the left inset of Fig. 5. For  $U < 5$  eV, a temperature-dependent peak appears at the chemical potential. Nevertheless, the metallic state is robust and the spectrum remains gapless up to the largest studied value of  $U = 8$  eV (not shown).

The VB spectra  $\text{NiSe}_2$  (Fig. 5) overall resemble the  $\text{NiS}_2$  ones with some quantitative differences, such as the shift of the high-energy shoulder to  $-6.5$  eV, also visible in the experimental data. As in  $\text{NiS}_2$ , we find the  $p_\sigma^*$  band at the bottom of the CB manifold. Comparison of the calculated CB spectrum to the BIS data is less satisfactory than in the case of  $\text{NiS}_2$ . In particular, the experimental 2 eV peak is not found in the calculation.

Bearing in mind that the Se-Se dimer length of 2.52 Å is overestimated, we have performed a reference calculation with a reduced dimer length of 2.37 Å (just below the ex-

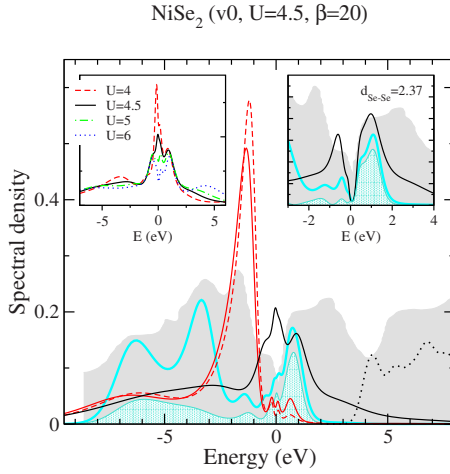


FIG. 5. (Color online) The calculated ( $U=4.5$  eV,  $T=580$  K) orbital resolved spectra of  $\text{NiSe}_2$  compared to the experimental XPS+BIS (Ref. 11) spectra (the same notation as in Fig. 3). The position of the calculated high-energy band is marked with the dotted line. Left inset shows the  $e_g^\sigma$  densities for various interaction strengths  $U$  (eV). In the right inset, the effect of reducing the Se-Se distance ( $\text{\AA}$ ) on the spectra ( $U=4.5$  eV) is shown.

perimental values). As shown in the right inset of Fig. 5, an increase of the dimer bonding-antibonding splitting leads to a strong suppression of the spectral density at the lowest energies (see the right inset of Fig. 5), but is not sufficient to open a charge gap. Since the bonding-antibonding splitting between the VB bottom and the  $p_\sigma^*$  peak is essentially a molecular property of the Se-Se dimer, it does not depend on the value of  $U$ .

### B. Origin of the charge gap

To analyze the behavior of the  $p_\sigma^*$  band, we have calculated the bare  $p$  band structures, obtained by decoupling the Ni- $d$  states. This can be done conveniently by removing the Ni-centered orbitals from the LDA basis set [Figs. 6(c) and 6(d)] or rigorously using the  $p$ - $p$  block of the Hamiltonian in Wannier basis [Figs. 6(a) and 6(b)] with qualitatively similar results. The  $p$  bands form a broad manifold bounded by dimer bonding bands at the bottom and a distinct antibonding  $p_\sigma^*$  band complex at the top, separated by a (pseudo) gap. The key difference between  $\text{NiS}_2$  and  $\text{NiSe}_2$  is the size of this gap separating the  $p_\sigma^*$  band from the rest of the  $p$  manifold controlled by the length of the dimer. The gap in  $\text{NiS}_2$  is large enough to survive the hybridization with the correlated Ni- $d$  orbitals, while the  $\text{NiSe}_2$  gap is too small and the coupling to  $d$  orbitals closes it completely.

Next, we consider the effect of applied pressure. The LDA+DMFT calculations for pressures up to 13 GPa show the closing of the charge gap (Fig. 7). This is a result of the combination of the rigidity of the S-S dimer and an overall band broadening. As a consequence of the former, the bonding-antibonding splitting is insensitive to pressure. On the other hand, the widths of the individual  $p$  bands, controlled by the reduced interdimer distances, increase with pressure thus reducing the bare  $p$  gap. Together with increas-

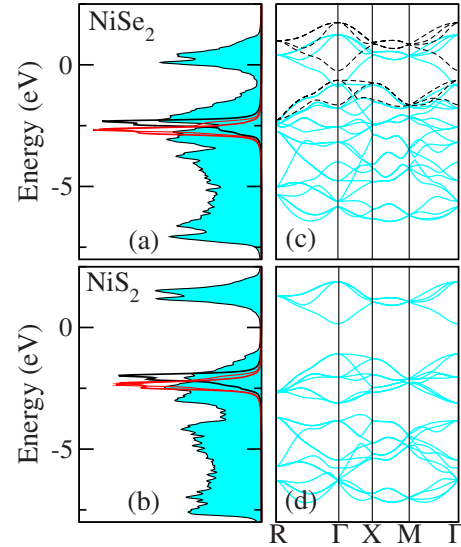


FIG. 6. (Color online) The bare S(Se)- $p$  spectral densities and band structures. [(a) and (b)] The spectral densities in the left panel are obtained from a Wannier function Hamiltonian, while [(c) and (d)] the band structures in the middle panel are based on a linearized augmented plane-wave (LAPW) calculation with removed Ni-like basis functions. Dashed bands for  $\text{NiSe}_2$  correspond to a reduced Se-Se distance.

ing  $p$ - $d$  hybridization, this leads to the metal-insulator transition. Noteworthy, the LDA results showed an elongation of the Se-Se dimer at moderate pressures, suggesting that the pressure-induced closing of the charge gap proceeds faster in compounds with higher Se content.

### C. IR reflectivity

To verify the theoretical conclusions and to obtain further information about the electronic properties of  $\text{NiS}_{2-x}\text{Se}_x$ , we

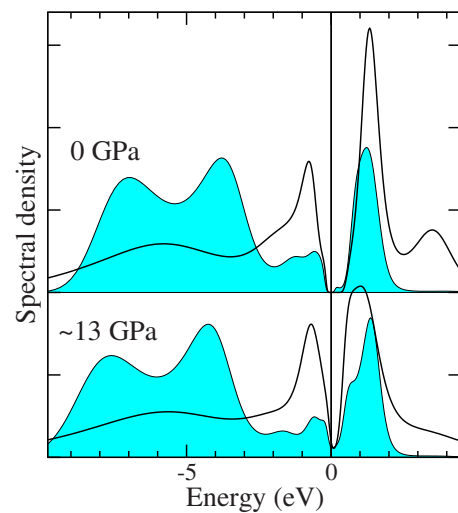


FIG. 7. (Color online) The comparison of  $\text{NiS}_2$  spectra in the insulating state at ambient pressure (upper panel) and in the metallic state under compression (lower panel). Black line marks the  $e_g^\sigma$  and shaded area (blue) is the total S  $p$  contribution. The  $t_{2g}$  spectra which exhibit very little change with pressure are not shown.

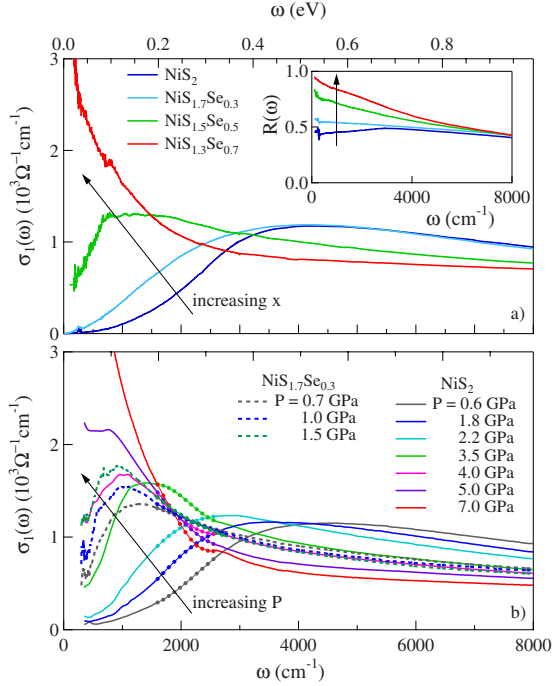


FIG. 8. (Color online) (a) Room-temperature optical conductivity spectra of  $\text{NiS}_{2-x}\text{Se}_x$  ( $x=0;0.3;0.5;0.7$ , as indicated in figure) at ambient pressure. In the inset, the corresponding reflectivity  $R(\omega)$  is reported. (b) Optical conductivity of  $\text{NiS}_2$  (solid) and  $\text{NiS}_{1.7}\text{Se}_{0.3}$  (dashed) for increasing pressure.

have measured the infrared properties of the  $\text{NiS}_{2-x}\text{Se}_x$  series ( $x=0;0.3;0.5;0.7$ ) at ambient conditions, shown in Fig. 8(a). For  $\text{NiS}_2$ ,  $R(\omega)$  slightly increases with increasing frequency, showing a broad maximum in the midinfrared and two narrow phonon absorptions in the far-IR. As Se is chemically substituted in the compound,  $R(\omega)$  increases its absolute value at low frequency, partially shielding the phonon lines and eventually becoming metalliclike (i.e., decreasing with increasing  $\omega$ ) for  $x=0.7$ . The corresponding optical conductivities  $\sigma_1(\omega)$  clearly show how the transition from an insulator ( $\text{NiS}_2$ ) to a metal ( $\text{NiS}_{1.3}\text{Se}_{0.7}$ ) takes place. A well-defined gap followed by an absorption band is found for  $\text{NiS}_2$ . As Se is introduced, the absorption band moves toward lower energies, progressively closing the gap.

A similar behavior is found as pressure is applied: as shown in Fig. 8(b), it is again the redshift of the absorption band that closes the gap. A closer inspection at the curve at 5 GPa for  $\text{NiS}_2$  shows the coexistence of two distinct terms at low frequency. As it was also shown in recent IR measurements,<sup>13</sup> our data can be fitted at low frequency with two distinct features: a Drude-like term and a Lorentz peak.

Our aim is to follow and compare the gap closure by chemical alloying and external pressure. We define the experimental optical gap as the frequency at half height of the absorption band and report its values in Fig. 9 for  $\text{NiS}_2$  and  $\text{NiS}_{1.7}\text{Se}_{0.3}$  under pressure. This definition of the gap leads to a similar pressure dependence as obtained by linearly extrapolating the steepest rise of  $\sigma_1(\omega)$  (Ref. 29) or by considering the maximum of the absorption peak obtained with Drude-Lorentz fitting.<sup>22</sup> We remark that strong phonon absorptions of the diamond prevent to have (fully) reliable data

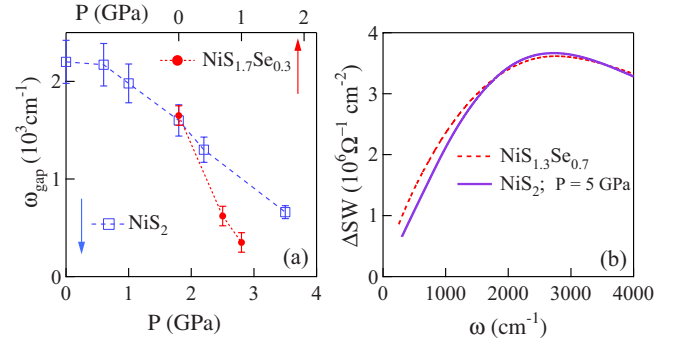


FIG. 9. (Color online) (a) The gap vs pressure for  $\text{NiS}_2$  and  $\text{NiS}_{1.7}\text{Se}_{0.3}$  (note the mutual horizontal offset). (b) SW transfer  $\Delta\text{SW}$  for  $\text{NiS}_2$  at 5 GPa and for  $\text{NiS}_{1.3}\text{Se}_{0.7}$  at ambient pressure.

between 1700 and 2500  $\text{cm}^{-1}$ . To overcome this problem and unambiguously define the gap value, the data analysis was performed as follows: reflectivity data are fitted with a Drude-Lorentz model in order to extrapolate the missing parts of the spectra. The Kramers-Kronig (KK) transformations are performed, followed by a simultaneous fitting of  $R$  and  $\sigma$ . This process is carried out iteratively until the  $\sigma_1(\omega)$  is stable with respect to the extrapolation used in the KK transformations.

Comparing the conductivity spectra, we find that the qualitatively similar effect of pressure on  $\text{NiS}_2$  and S substitution by Se follows the scaling relation  $P[\text{GPa}] \approx x/0.15$  proposed in Ref. 4. The pressure dependence of the optical gaps for pure  $\text{NiS}_2$  and  $\text{NiS}_{1.7}\text{Se}_{0.3}$  is shown in Fig. 9(a), with a horizontal offset according to the scaling relation. Our experimental results show that in the Se-doped compound, pressure is more efficient in closing the gap, in accordance with the previous theoretical reasoning.

Next we discuss the metallic phase. To quantify the “metallicity,” we use the spectral weight (SW) transfer relative to the ambient pressure  $\text{NiS}_2$  data  $\Delta\text{SW} = \text{SW}(x, P) - \text{SW}(x=0, P=0)$ , where  $\text{SW}(\omega) = \int_0^\omega \sigma_1(\omega') d\omega'$ . Recalling that at low frequency there is the coexistence of two terms, we can infer that with applied pressure, a large part of the spectral weight is transferred to the mid-IR region first, while the appearance of Drude-like peak occurs upon further pressure increase [see Fig. 8(b)]. Without making a quantitative connection, we point out that a qualitatively similar behavior is observed in the DMFT results. As pressure is applied to  $\text{NiS}_2$ , due to the rigidity of the S-S dimers, the transition occurs mainly due to band broadening not corresponding at first instance to the formation of a Drude term. Instead, when the Se-Se distance is varied, we expect a fast response of the low-energy electrodynamics (right inset of Fig. 5). Following the scaling relation, we compare  $\text{NiS}_2$  at 5 GPa with  $\text{NiS}_{1.3}\text{Se}_{0.7}$  at ambient pressure in Fig. 9(b). Although a similar amount of SW is transferred below 4000  $\text{cm}^{-1}$ ,  $\text{NiS}_{1.3}\text{Se}_{0.7}$  exhibits a higher SW transfer at lower frequencies ( $<2000 \text{ cm}^{-1}$ ) pointing to a more intense Drude-like term, also supporting our conclusion about the faster onset of metallicity with Se substitution.

## V. CONCLUSIONS

Using the LDA+DMFT approach, we have reproduced the paramagnetic phases of  $\text{NiS}_2$  (insulator) and  $\text{NiSe}_2$

(metal) and provide the following answers to the questions posed in the introduction: (i) The presence of the charge gap in NiS<sub>2</sub> in contrast to NiSe<sub>2</sub> is a consequence of a larger gap in the bare  $p$  band structure ( $p$  gap) of NiS<sub>2</sub> resulting from stronger bonding within the S-S dimer. (ii) The pressure reduces the  $p$  gap by broadening the individual  $p$  bands, while the Se substitution reduces the  $p$  gap due to smaller bonding-antibonding splitting. (iii) The MIT is controlled by varying the size of the  $p$  gap. We find both computationally and experimentally that the pressure driven MIT is accelerated by the Se substitution. The conceptual picture of NiS<sub>2-x</sub>Se<sub>x</sub> is provided by a periodic Anderson model with a variable gap in the conduction-electron bath rather than the charge-transfer insulator model.

#### ACKNOWLEDGMENTS

We thank P. Werner for providing his quantum Monte Carlo code, D. Vollhardt for critical reading of an early version of the paper, and C. Schuster for useful discussions.

L.B., K.R., and C.A.K. thank B. Gasharova, Y.-L. Mathis, D. Moss, and M. Süpfle for help at the IR beamline and H. Takagi for kindly providing the samples. We acknowledge the financial support of SFB 484 of the Deutsche Forschungsgemeinschaft (J.K., L.B., C.A.K., and K.R.), Fondazione della Riccia (L.B.), Bayerische Forschungsstiftung (L.B. and R.K.), and Russian Foundation for Basic Research under Grant No. RFFI-07-02-00041, Dynasty Foundation, President of Russian Federation Fund Grant No. NSH 1941.2008.2, and Program of Russian Academy of Science Presidium “Quantum microphysics of condensed matter” N7 (Dm. M.K and V.I.A.), beam time provided by ANKA Angströmquelle Karlsruhe, and computer time provided by Leibniz Supercomputing Center Munich. J.A.M., E.Z.K, and A.M. acknowledge support of the Research Council of the President of the Russian Federation (Grant No. NSH-3572.2010.2), the Russian Science Foundation for Basic Research (Project No. 08-02-00148), the Natural Sciences and Engineering Research Council of Canada (NSERC), and the Canada Research Chair program.

\*kunes@fzu.cz

- <sup>1</sup>P. Kwizera, M. S. Dresselhaus, and D. Adler, *Phys. Rev. B* **21**, 2328 (1980).
- <sup>2</sup>X. Yao, J. M. Honig, T. Hogan, C. Kannewurf, and J. Spätek, *Phys. Rev. B* **54**, 17469 (1996).
- <sup>3</sup>M. Matsuura, H. Hiraka, K. Yamada, and Y. Endoh, *J. Phys. Soc. Jpn.* **69**, 1503 (2000).
- <sup>4</sup>S. Miyasaka, H. Takagi, Y. Sekine, H. Takahashi, N. Mori, and R. J. Cava, *J. Phys. Soc. Jpn.* **69**, 3166 (2000).
- <sup>5</sup>N. Takeshita, S. Takashima, C. Terakura, H. Nishikubo, S. Miyasaka, M. Nohara, Y. Tokura, and H. Takagi, arXiv:0704.0591 (unpublished).
- <sup>6</sup>A. Georges, G. Kotliar, W. Krauth, and M. J. Rozenberg, *Rev. Mod. Phys.* **68**, 13 (1996).
- <sup>7</sup>A. Fujimori, K. Mamiya, T. Mizokawa, T. Miyadai, T. Sekiguchi, H. Takahashi, N. Mori, and S. Suga, *Phys. Rev. B* **54**, 16329 (1996).
- <sup>8</sup>A. Y. Matsuura, Z. X. Shen, D. S. Dessau, C. H. Park, T. Thio, J. W. Bennett, and O. Jepsen, *Phys. Rev. B* **53**, R7584 (1996).
- <sup>9</sup>D. D. Sarma, M. Pedio, M. Capozzi, A. Girycki, N. Chandrasekharan, N. Shanthi, S. R. Krishnakumar, C. Ottaviani, C. Quaresima, and P. Perfetti, *Phys. Rev. B* **57**, 6984 (1998).
- <sup>10</sup>E. K. Li, K. H. Johnson, D. E. Eastman, and J. L. Freeouf, *Phys. Rev. Lett.* **32**, 470 (1974).
- <sup>11</sup>W. Folkerts, G. A. Sawatzky, C. Haas, R. A. de Groot, and F. U. Hillebrecht, *J. Phys. C* **20**, 4135 (1987).
- <sup>12</sup>D. W. Bullett, *J. Phys. C* **15**, 6163 (1982).
- <sup>13</sup>A. Perucchi *et al.*, *Phys. Rev. B* **80**, 073101 (2009).
- <sup>14</sup>J. Zaanen, G. A. Sawatzky, and J. W. Allen, *Phys. Rev. Lett.* **55**, 418 (1985).
- <sup>15</sup>K. Held, I. A. Nekrasov, G. Keller, V. Eyert, N. Blümer, A. K. McMahan, R. T. Scalettar, T. Pruschke, V. I. Anisimov, and D. Vollhardt, *Phys. Status Solidi B* **243**, 2599 (2006).
- <sup>16</sup>P. Blaha, K. Schwarz, G. K. H. Madsen, D. Kvasnicka, and J. Luitz, *WIEN2K, An Augmented Plane Wave+Local Program for Calculating Crystal Properties* (Technical University Wien, Austria, 2001).
- <sup>17</sup>D. M. Korotin, A. V. Kozhevnikov, S. L. Skornyakov, I. Leonov, N. Binggeli, V. I. Anisimov, and G. Trimarchi, *Eur. Phys. J. B* **65**, 91 (2008).
- <sup>18</sup>S. Baroni *et al.*, <http://www.pwscf.org/>
- <sup>19</sup>J. Kuneš, D. M. Korotin, M. A. Korotin, V. I. Anisimov, and P. Werner, *Phys. Rev. Lett.* **102**, 146402 (2009).
- <sup>20</sup>P. Werner, A. Comanac, L. de Medici, M. Troyer, and A. J. Millis, *Phys. Rev. Lett.* **97**, 076405 (2006).
- <sup>21</sup>M. Jarrell and J. E. Gubernatis, *Phys. Rep.* **269**, 133 (1996).
- <sup>22</sup>F. Wooten, *Optical Properties of Solids* (Academic Press, New York, 1972).
- <sup>23</sup>H. K. Mao, J. Xu, and P. M. Bell, *J. Geophys. Res.* **91**, 4673 (1986).
- <sup>24</sup>A. Pashkin, M. Dressel, and C. A. Kuntscher, *Phys. Rev. B* **74**, 165118 (2006).
- <sup>25</sup>L. Baldassarre, A. Perucchi, E. Arcangeletti, D. Nicoletti, D. Di Castro, P. Postorino, V. A. Sidorov, and S. Lupi, *Phys. Rev. B* **75**, 245108 (2007).
- <sup>26</sup>J. Kuneš, V. I. Anisimov, A. V. Lukoyanov, and D. Vollhardt, *Phys. Rev. B* **75**, 165115 (2007).
- <sup>27</sup>R. Otero, J. L. M. deVidales, and C. de las Heras, *J. Phys.: Condens. Matter* **10**, 6919 (1998).
- <sup>28</sup>C. Sugiura, I. Suzuki, J. Kashiwakura, and Y. Gohshi, *J. Phys. Soc. Jpn.* **40**, 1720 (1976).
- <sup>29</sup>T. Katsufuji, Y. Okimoto, and Y. Tokura, *Phys. Rev. Lett.* **75**, 3497 (1995).